EUROPEAN ORGANIZATION FOR NUCLEAR RESEARCH

CERN–PPE/94-193

29 November 1994

Measurement of the Forward-Backward Asymmetry of charm and bottom Quarks at the Z Pole using $D^{*\pm}$ Mesons

DELPHI Collaboration

Abstract

The forward-backward asymmetries for the processes $e^+e^- \to c\bar{c}$ and $e^+e^- \to b\bar{b}$ at the Z resonance are measured using identified $D^{*\pm}$ mesons. In 905,000 selected hadronic events, taken in 1991 and 1992 with the DELPHI detector at LEP, 4757 $D^{*+} \to D^\circ\pi^+$ decays are reconstructed. The c and b quark forward-backward asymmetries are determined to be:

$$\begin{aligned} A_{FB}^{c\bar{c}} &= 0.077 \pm 0.029\,(\text{stat}) \pm 0.012\,(\text{sys}) \ , \\ A_{FB}^{b\bar{b}} &= 0.059 \pm 0.062\,(\text{stat}) \pm 0.024\,(\text{sys}) \ . \end{aligned}$$

Constraining the b asymmetry to the value measured by DELPHI using independent analyses, the charm asymmetry is determined to be:

$$A_{FB}^{c,const} = 0.068 \pm 0.027\,(\text{stat}) \pm 0.011\,(\text{sys}) \ .$$

This result corresponds to an effective electroweak mixing angle measured using charm quark events of:

$$\sin^2\theta_{eff}^{lept} = 0.2307 \pm 0.0062\,(\text{stat}) \pm 0.0026\,(\text{sys}) \ .$$

(To be submitted to Zeit. f. Physik C)

P.Abreu[21], W.Adam[8], T.Adye[38], E.Agasi[31], I.Ajinenko[43], R.Aleksan[40], G.D.Alekseev[15], P.P.Allport[22], S.Almehed[24], F.M.L.Almeida[48], S.J.Alvsvaag[4], U.Amaldi[8], A.Andreazza[28], M.L.Andrieux[13], P.Antilogus[25], W-D.Apel[16], Y.Arnoud[40], B.Åsman[45], J-E.Augustin[19], A.Augustinus[31], P.Baillon[8], P.Bambade[19], F.Barao[21], R.Barate[13], D.Y.Bardin[15], G.J.Barker[35], A.Baroncelli[41], O.Barring[8], J.A.Barrio[26], W.Bartl[51], M.J.Bates[38], M.Battaglia[14], M.Baubillier[23], J.Baudot[40], K-H.Becks[53], M.Begalli[37], P.Beilliere[7], Yu.Belokopytov[8], P.Beltran[10], A.C.Benvenuti[5], M.Berggren[42], D.Bertrand[2], F.Bianchi[46], M.Bigi[46], M.S.Bilenky[15], P.Billoir[23], J.Bjarne[24], D.Bloch[9], M.Blume[53], S.Blyth[35], V.Bocci[39], T.Bolognese[40], M.Bonesini[28], W.Bonivento[28], P.S.L.Booth[22], G.Borisov[43], C.Bosio[41], B.Bostjancic[44], S.Bosworth[35], O.Botner[49], B.Bouquet[19], C.Bourdarios[19], T.J.V.Bowcock[22], M.Bozzo[12], P.Branchini[41], K.D.Brand[36], R.A.Brenner[14], H.Briand[23], C.Bricman[2], L.Brillault[23], R.C.A.Brown[8], P.Bruckman[17], J-M.Brunet[7], L.Bugge[33], T.Buran[33], A.Buys[8], M.Caccia[28], M.Calvi[28], A.J.Camacho Rozas[42], T.Camporesi[8], V.Canale[39], M.Canepa[12], K.Cankocak[45], F.Cao[2], F.Carena[8], P.Carrilho[48], L.Carroll[22], C.Caso[12], V.Cassio[46], M.V.Castillo Gimenez[50], A.Cattai[8], F.R.Cavallo[5], L.Cerrito[39], V.Chabaud[8], A.Chan[1], Ph.Charpentier[8], L.Chaussard[25], J.Chauveau[23], P.Checchia[36], G.A.Chelkov[15], P.Chliapnikov[43], P.Chochula[6], V.Chorowicz[8], J.T.M.Chrin[50], V.Cindro[44], P.Collins[35], J.L.Contreras[19], R.Contri[12], E.Cortina[50], G.Cosme[19], F.Cossutti[47], F.Couchot[19], H.B.Crawley[1], D.Crennell[38], G.Crosetti[12], J.Cuevas Maestro[34], S.Czellar[14], E.Dahl-Jensen[29], J.Dahm[53], B.Dalmagne[19], M.Dam[33], G.Damgaard[29], A.Daum[16], P.D.Dauncey[38], M.Davenport[8], W.Da Silva[23], C.Defoix[7], G.Dellaricca[47], G.Della Ricca[47], P.Delpierre[27], N.Demaria[35], A.De Angelis[8], H.De Boeck[2], W.De Boer[16], S.De Brabandere[2], C.De Clercq[2], M.D.M.De Fez Laso[50], C.De La Vaissiere[23], B.De Lotto[47], A.De Min[28], L.De Paula[48], C.De Saint-Jean[40], H.Dijkstra[8], L.Di Ciaccio[39], F.Djama[9], J.Dolbeau[7], M.Donszelmann[8], K.Doroba[52], M.Dracos[9], J.Drees[53], K.-A.Drees[53], M.Dris[32], Y.Dufour[7], F.Dupont[13], D.Edsall[1], R.Ehret[16], T.Ekelof[49], G.Ekspong[45], M.Elsing[53], J-P.Engel[9], N.Ershaidat[23], M.Espirito Santo[21], D.Fassouliotis[32], M.Feindt[8], A.Fenyuk[43], A.Ferrer[50], T.A.Filippas[32], A.Firestone[1], H.Foeth[8], E.Fokitis[32], F.Fontanelli[12], F.Formenti[8], J-L.Fousset[27], B.Franek[38], P.Frenkiel[7], D.C.Fries[16], A.G.Frodesen[4], R.Fruhwirth[51], F.Fulda-Quenzer[19], H.Furstenau[8], J.Fuster[8], D.Gamba[46], M.Gandelman[18], C.Garcia[50], J.Garcia[42], C.Gaspar[8], U.Gasparini[36], Ph.Gavillet[8], E.N.Gazis[32], D.Gele[9], J-P.Gerber[9], D.Gillespie[8], R.Gokieli[52], B.Golob[44], J.J.Gomez Y Cadenas[8], G.Gopal[38], L.Gorn[1], M.Gorski[52], V.Gracco[12], F.Grard[2], E.Graziani[41], G.Grosdidier[19], P.Gunnarsson[45], J.Guy[38], U.Haedinger[16], F.Hahn[53], M.Hahn[16], S.Hahn[53], S.Haider[31], Z.Hajduk[17], A.Hakansson[24], A.Hallgren[49], K.Hamacher[53], W.Hao[31], F.J.Harris[35], V.Hedberg[24], R.Henriques[21], J.J.Hernandez[50], J.A.Hernando[50], P.Herquet[2], H.Herr[8], T.L.Hessing[8], E.Higon[50], H.J.Hilke[8], T.S.Hill[1], S-O.Holmgren[45], P.J.Holt[35], D.Holthuizen[31], P.F.Honore[7], M.Houlden[22], J.Hrubec[51], K.Huet[2], K.Hultqvist[45], P.Ioannou[3], P-S.Iversen[4], J.N.Jackson[22], R.Jacobsson[45], P.Jalocha[17], R.Janik[6], G.Jarlskog[24], P.Jarry[40], B.Jean-Marie[19], E.K.Johansson[45], L.Jonsson[24], P.Juillot[9], M.Kaiser[16], G.Kalmus[38], F.Kapusta[23], M.Karlsson[45], E.Karvelas[10], A.Katargin[43], S.Katsanevas[3], E.C.Katsoufis[32], R.Keranen[14], B.A.Khomenko[15], N.N.Khovanski[15], B.King[22], N.J.Kjaer[29], H.Klein[8], A.Klovning[4], P.Kluit[31], J.H.Koehne[16], B.Koene[31], P.Kokkinias[10], M.Koratzinos[8], V.Kostioukhine[43], C.Kourkoumelis[3], O.Kouznetsov[12], P.-H.Kramer[53], M.Krammer[51], C.Kreuter[16], J.Krolikowski[52], I.Kronkvist[24], Z.Krumstein[15], W.Krupinski[17], P.Kubinec[6], W.Kucewicz[17], K.Kulka[49], K.Kurvinen[14], C.Lacasta[50], I.Laktineh[25], C.Lambropoulos[10], J.W.Lamsa[1], L.Lanceri[47], P.Langefeld[53], V.Lapin[43], I.Last[22], J-P.Laugier[40], R.Lauhakangas[14], G.Leder[51], F.Ledroit[13], V.Lefebure[2], R.Leitner[30], Y.Lemoigne[40], J.Lemonne[2], G.Lenzen[53], V.Lepeltier[19], T.Lesiak[36], J.M.Levy[9], D.Liko[51], R.Lindner[53], A.Lipniacka[19], I.Lippi[36], B.Loerstad[24], M.Lokajicek[11], J.G.Loken[35], A.Lopez-Fernandez[8], M.A.Lopez Aguera[42], D.Loukas[10], J.J.Lozano[50], P.Lutz[40], L.Lyons[35], G.Maehlum[16], J.Maillard[7], A.Maio[21], A.Maltezos[10], V.Malychev[15], F.Mandl[51], J.Marco[42], B.Marechal[48], M.Margoni[36], J-C.Marin[8], C.Mariotti[41], A.Markou[10], T.Maron[53], C.Martinez-Rivero[42], F.Martinez-Vidal[50], S.Marti i Garcia[50], F.Matorras[42], C.Matteuzzi[28], G.Matthiae[39], M.Mazzucato[36], M.Mc Cubbin[8], R.Mc Kay[1], R.Mc Nulty[22], J.Medbo[49], C.Meroni[28], W.T.Meyer[1], M.Michelotto[36], E.Migliore[46], I.Mikulec[51], L.Mirabito[25], W.A.Mitaroff[51], U.Mjoernmark[24], T.Moa[45], R.Moeller[29], K.Moenig[8], M.R.Monge[12], P.Morettini[12], H.Mueller[16], W.J.Murray[38], B.Muryn[17], G.Myatt[35], F.Naraghi[13], F.L.Navarria[5], S.Navas[50], P.Negri[28], S.Nemecek[11], W.Neumann[53], N.Neumeister[51], R.Nicolaidou[3], B.S.Nielsen[29], V.Nikolaenko[25], P.Niss[45], A.Nomerotski[36], A.Normand[35], W.Oberschulte-Beckmann[16], V.Obraztsov[43], A.G.Olshevski[15], R.Orava[14], K.Osterberg[14], A.Ouraou[40], P.Paganini[19], M.Paganoni[28], R.Pain[23], H.Palka[17], Th.D.Papadopoulou[32], L.Pape[8], F.Parodi[12], A.Passeri[41], M.Pegoraro[36], J.Pennanen[14], L.Peralta[21], V.Perevozchikov[43], H.Pernegger[51], A.Perrotta[5], C.Petridou[47], A.Petrolini[12], H.T.Phillips[38], G.Piana[12], F.Pierre[40], M.Pimenta[21], S.Plaszczynski[19], O.Podobrin[16], M.E.Pol[18], G.Polok[17], P.Poropat[47], V.Pozdniakov[15], M.Prest[47], P.Privitera[39], A.Pullia[28], D.Radojicic[35], S.Ragazzi[28], H.Rahmani[32], J.Rames[11], P.N.Ratoff[20], A.L.Read[33], M.Reale[53], P.Rebecchi[19], N.G.Redaelli[28], M.Regler[51], D.Reid[8], P.B.Renton[35], L.K.Resvanis[3], F.Richard[19], J.Richardson[22], J.Ridky[11], G.Rinaudo[46], I.Ripp[40], A.Romero[46], I.Roncagliolo[12], P.Ronchese[36], V.Ronjin[43], L.Roos[13], E.I.Rosenberg[1], E.Rosso[8], P.Roudeau[19], T.Rovelli[5], W.Ruckstuhl[31], V.Ruhlmann-Kleider[40], A.Ruiz[42], H.Saarikko[14], Y.Sacquin[40], A.Sadovsky[15],

G.Sajot[13], J.Salt[50], J.Sanchez[26], M.Sannino[12], H.Schneider[16], M.A.E.Schyns[53], G.Sciolla[46], F.Scuri[47], Y.Sedykh[15], A.M.Segar[35], A.Seitz[16], R.Sekulin[38], R.C.Shellard[37], I.Siccama[31], P.Siegrist[40], S.Simonetti[40], F.Simonetto[36], A.N.Sisakian[15], B.Sitar[6], T.B.Skaali[33], G.Smadja[25], N.Smirnov[43], O.Smirnova[15], G.R.Smith[38], R.Sosnowski[52], D.Souza-Santos[37], T.Spassov[21], E.Spiriti[41], S.Squarcia[12], H.Staeck[53], C.Stanescu[41], S.Stapnes[33], I.Stavitski[36], G.Stavropoulos[10], K.Stepaniak[52], F.Stichelbaut[8], A.Stocchi[19], J.Strauss[51], R.Strub[9], B.Stugu[4], M.Szczekowski[52], M.Szeptycka[52], T.Tabarelli[28], O.Tchikilev[43], G.E.Theodosiou[10], Z.Thome[48], A.Tilquin[27], J.Timmermans[31], L.G.Tkatchev[15], T.Todorov[9], D.Z.Toet[31], A.Tomaradze[2], B.Tome[21], E.Torassa[46], L.Tortora[41], G.Transtromer[24], D.Treille[8], W.Trischuk[8], G.Tristram[7], C.Troncon[28], A.Tsirou[8], M-L.Turluer[40], T.Tuuva[14], I.A.Tyapkin[23], M.Tyndel[38], S.Tzamarias[22], B.Ueberschaer[53], S.Ueberschaer[53], O.Ullaland[8], G.Valenti[5], E.Vallazza[8], J.A.Valls Ferrer[50], C.Vander Velde[2], G.W.Van Apeldoorn[31], P.Van Dam[31], W.K.Van Doninck[2], J.Van Eldik[31], G.Vegni[28], L.Ventura[36], W.Venus[38], F.Verbeure[2], M.Verlato[36], L.S.Vertogradov[15], D.Vilanova[40], P.Vincent[25], L.Vitale[47], E.Vlasov[43], A.S.Vodopyanov[15], M.Voutilainen[14], V.Vrba[11], H.Wahlen[53], C.Walck[45], F.Waldner[47], A.Wehr[53], M.Weierstall[53], P.Weilhammer[8], A.M.Wetherell[8], D.Wicke[53], J.H.Wickens[2], M.Wielers[16], G.R.Wilkinson[35], W.S.C.Williams[35], M.Winter[9], M.Witek[8], G.Wormser[19], K.Woschnagg[49], K.Yip[35], O.Yushchenko[43], F.Zach[25], A.Zaitsev[43], A.Zalewska[17], P.Zalewski[52], D.Zavrtanik[44], E.Zevgolatakos[10], N.I.Zimin[15], M.Zito[40], D.Zontar[44], R.Zuberi[35], G.C.Zucchelli[45], G.Zumerle[36]

[1] Ames Laboratory and Department of Physics, Iowa State University, Ames IA 50011, USA
[2] Physics Department, Univ. Instelling Antwerpen, Universiteitsplein 1, B-2610 Wilrijk, Belgium
and IIHE, ULB-VUB, Pleinlaan 2, B-1050 Brussels, Belgium
and Faculté des Sciences, Univ. de l'Etat Mons, Av. Maistriau 19, B-7000 Mons, Belgium
[3] Physics Laboratory, University of Athens, Solonos Str. 104, GR-10680 Athens, Greece
[4] Department of Physics, University of Bergen, Allégaten 55, N-5007 Bergen, Norway
[5] Dipartimento di Fisica, Università di Bologna and INFN, Via Irnerio 46, I-40126 Bologna, Italy
[6] Comenius University, Faculty of Mathematics and Physics, Mlynska Dolina, SK-84215 Bratislava, Slovakia
[7] Collège de France, Lab. de Physique Corpusculaire, IN2P3-CNRS, F-75231 Paris Cedex 05, France
[8] CERN, CH-1211 Geneva 23, Switzerland
[9] Centre de Recherche Nucléaire, IN2P3 - CNRS/ULP - BP20, F-67037 Strasbourg Cedex, France
[10] Institute of Nuclear Physics, N.C.S.R. Demokritos, P.O. Box 60228, GR-15310 Athens, Greece
[11] FZU, Inst. of Physics of the C.A.S. High Energy Physics Division, Na Slovance 2, 180 40, Praha 8, Czech Republic
[12] Dipartimento di Fisica, Università di Genova and INFN, Via Dodecaneso 33, I-16146 Genova, Italy
[13] Institut des Sciences Nucléaires, IN2P3-CNRS, Université de Grenoble 1, F-38026 Grenoble Cedex, France
[14] Research Institute for High Energy Physics, SEFT, P.O. Box 9, FIN-00014 Helsinki, Finland
[15] Joint Institute for Nuclear Research, Dubna, Head Post Office, P.O. Box 79, 101 000 Moscow, Russian Federation
[16] Institut für Experimentelle Kernphysik, Universität Karlsruhe, Postfach 6980, D-76128 Karlsruhe, Germany
[17] High Energy Physics Laboratory, Institute of Nuclear Physics, Ul. Kawiory 26a, PL-30055 Krakow 30, Poland
[18] Centro Brasileiro de Pesquisas Físicas, rua Xavier Sigaud 150, BR-22290 Rio de Janeiro, Brazil
[19] Université de Paris-Sud, Lab. de l'Accélérateur Linéaire, IN2P3-CNRS, Bat 200, F-91405 Orsay Cedex, France
[20] School of Physics and Materials, University of Lancaster, Lancaster LA1 4YB, UK
[21] LIP, IST, FCUL - Av. Elias Garcia, 14-1°, P-1000 Lisboa Codex, Portugal
[22] Department of Physics, University of Liverpool, P.O. Box 147, Liverpool L69 3BX, UK
[23] LPNHE, IN2P3-CNRS, Universités Paris VI et VII, Tour 33 (RdC), 4 place Jussieu, F-75252 Paris Cedex 05, France
[24] Department of Physics, University of Lund, Sölvegatan 14, S-22363 Lund, Sweden
[25] Université Claude Bernard de Lyon, IPNL, IN2P3-CNRS, F-69622 Villeurbanne Cedex, France
[26] Universidad Complutense, Avda. Complutense s/n, E-28040 Madrid, Spain
[27] Univ. d'Aix - Marseille II - CPP, IN2P3-CNRS, F-13288 Marseille Cedex 09, France
[28] Dipartimento di Fisica, Università di Milano and INFN, Via Celoria 16, I-20133 Milan, Italy
[29] Niels Bohr Institute, Blegdamsvej 17, DK-2100 Copenhagen 0, Denmark
[30] NC, Nuclear Centre of MFF, Charles University, Areal MFF, V Holesovickach 2, 180 00, Praha 8, Czech Republic
[31] NIKHEF-H, Postbus 41882, NL-1009 DB Amsterdam, The Netherlands
[32] National Technical University, Physics Department, Zografou Campus, GR-15773 Athens, Greece
[33] Physics Department, University of Oslo, Blindern, N-1000 Oslo 3, Norway
[34] Dpto. Fisica, Univ. Oviedo, C/P. Pérez Casas, S/N-33006 Oviedo, Spain
[35] Department of Physics, University of Oxford, Keble Road, Oxford OX1 3RH, UK
[36] Dipartimento di Fisica, Università di Padova and INFN, Via Marzolo 8, I-35131 Padua, Italy
[37] Depto. de Fisica, Pontificia Univ. Católica, C.P. 38071 RJ-22453 Rio de Janeiro, Brazil
[38] Rutherford Appleton Laboratory, Chilton, Didcot OX11 OQX, UK
[39] Dipartimento di Fisica, Università di Roma II and INFN, Tor Vergata, I-00173 Rome, Italy
[40] Centre d'Etude de Saclay, DSM/DAPNIA, F-91191 Gif-sur-Yvette Cedex, France
[41] Istituto Superiore di Sanità, Ist. Naz. di Fisica Nucl. (INFN), Viale Regina Elena 299, I-00161 Rome, Italy
[42] C.E.A.F.M., C.S.I.C. - Univ. Cantabria, Avda. los Castros, S/N-39006 Santander, Spain, (CICYT-AEN93-0832)
[43] Inst. for High Energy Physics, Serpukov P.O. Box 35, Protvino, (Moscow Region), Russian Federation
[44] J. Stefan Institute and Department of Physics, University of Ljubljana, Jamova 39, SI-61000 Ljubljana, Slovenia
[45] Fysikum, Stockholm University, Box 6730, S-113 85 Stockholm, Sweden
[46] Dipartimento di Fisica Sperimentale, Università di Torino and INFN, Via P. Giuria 1, I-10125 Turin, Italy
[47] Dipartimento di Fisica, Università di Trieste and INFN, Via A. Valerio 2, I-34127 Trieste, Italy
and Istituto di Fisica, Università di Udine, I-33100 Udine, Italy
[48] Univ. Federal do Rio de Janeiro, C.P. 68528 Cidade Univ., Ilha do Fundão BR-21945-970 Rio de Janeiro, Brazil
[49] Department of Radiation Sciences, University of Uppsala, P.O. Box 535, S-751 21 Uppsala, Sweden
[50] IFIC, Valencia-CSIC, and D.F.A.M.N., U. de Valencia, Avda. Dr. Moliner 50, E-46100 Burjassot (Valencia), Spain
[51] Institut für Hochenergiephysik, Österr. Akad. d. Wissensch., Nikolsdorfergasse 18, A-1050 Vienna, Austria
[52] Inst. Nuclear Studies and University of Warsaw, Ul. Hoza 69, PL-00681 Warsaw, Poland
[53] Fachbereich Physik, University of Wuppertal, Postfach 100 127, D-42097 Wuppertal 1, Germany

1 Introduction

The cross section for the process $e^+e^- \to f\bar{f}$ for the fermion f as a function of the polar angle θ with respect to the direction of the e^- can be expressed as:

$$\frac{d\sigma}{d\cos\theta} \propto 1 + \frac{8}{3} A_{FB}^{f\bar{f}} \cos\theta + \cos^2\theta$$

The term proportional to $\cos\theta$ generates a forward-backward asymmetry, which in the framework of the Standard Model arises from the parity violation coupling structure of electroweak interactions. The forward-backward asymmetry $A_{FB}^{f\bar{f}}$ at the Z resonance results from the interference of the vector (v) and axial vector (a) couplings of the initial and final state fermions to the Z boson. The Born level asymmetry for pure Z exchange is given by:

$$A_{FB}^{f\bar{f}} = \frac{3}{4} \cdot \frac{2v_e a_e}{v_e^2 + a_e^2} \cdot \frac{2v_f a_f}{v_f^2 + a_f^2} \ . \tag{1}$$

This tree level relation is modified by higher order corrections. In the Improved Born approximation effective couplings $\bar{v}$ and $\bar{a}$ are used to account for electroweak corrections depending on the mass of the top quark and the Higgs boson. The ratio of the effective vector and axial vector couplings defines the effective electroweak mixing angle $\sin^2\theta_{eff}^f$:

$$\sin^2\theta_{eff}^f = \frac{1}{4|Q_f|}\left(1 - \frac{\bar{v}_f}{\bar{a}_f}\right) \ , \tag{2}$$

where Q_f is the electric charge of the fermion. A measurement of $A_{FB}^{f\bar{f}}$ is very sensitive to $\sin^2\theta_{eff}^f$ and allows a precise test of the Standard Model. For all fermions except b quarks, the differences predicted by the Standard Model between the $\sin^2\theta_{eff}^f$ are much smaller than the experimental errors and will therefore be called $\sin^2\theta_{eff}^{lept}$ in the following.

In this analysis, the forward-backward asymmetries for the processes $e^+e^- \to c\bar{c}$ and $e^+e^- \to b\bar{b}$ at $\sqrt{s} = M_Z$ are measured using reconstructed D^{*+} mesons [†]. The D^{*+} carries a charm quark and therefore provides a clean signature of a $c\bar{c}$ event or a decay of a heavy B meson in a $b\bar{b}$ event. In both cases the charge of the D^{*+} is directly correlated to the charge of the primary quark. A D^{*+} is identified through its decay into $D^\circ\pi^+$, while the D° is reconstructed in the decay modes $K^-\pi^+$, $K^-\pi^+(\pi^\circ)$ and $K^-\pi^+\pi^-\pi^+$. The energy of the D^{*+} and the decay length of the D° are used to separate $c\bar{c}$ and $b\bar{b}$ events. Particle identification, provided by the DELPHI Ring Imaging Cherenkov Counters (RICH) and the Time Projection Chamber (TPC), is used to reduce the combinatorial background.

After a short description of the D^{*+} reconstruction technique and the particle identification methods, the measurement of the forward-backward asymmetries with an unbinned maximum likelihood fit to the D^{*+} spectra, including the time dependence of the $B_d^\circ - \bar{B}_d^\circ$ mixing effect [1], is described below.

2 Detector description and event selection

This analysis uses charged particles measured with the tracking system of DELPHI. Here the components relevant to this analysis are briefly described. A detailed description of the DELPHI apparatus has been presented in [2].

[†] Throughout the paper charge-conjugated states are implicitly included.

The main part of the tracking system is a 2.7 m long TPC, which measures the tracks of charged particles with a precision of 250 μm in the $R\phi$ projection (transverse to the beam direction) and 0.9 mm along the z direction (beam direction). For particle identification, the 80% truncated mean of the amplitudes on up to 192 sense wires is used to measure the energy loss per unit of length (dE/dx).

The space between the TPC and the beam pipe contains the Inner Detector (ID) and the silicon microstrip Vertex Detector (VD). Each 15° sector of the ID consists of a 24 wire jet chamber with a precision of 70 μm in $R\phi$, followed by a 5 layer proportional chamber with 192 cathode strips per layer, providing a z measurement with a typical precision of 600 μm. The VD is built from three concentric shells of 24 silicon microstrip detector modules each 24 cm long. Each microstrip has a spatial precision of 7 μm in the $R\phi$ plane. The VD is therefore the most important detector component of DELPHI for reconstructing vertices.

In the barrel region (polar angle θ relative to the beam axis between 43° and 137°) the quality of tracking is further improved by the Outer Detector (OD) containing 5 layers of drift tubes. The OD measures the $R\phi$ coordinate with a precision of about 110 μm. Three layers also provide an approximate z measurement.

The Barrel RICH, mounted between the TPC and OD, covers a polar angle between 47° and 133°. It identifies charged particles by measuring the angle of emission of Cherenkov light, and thus the velocity. The mass of the charged particle is then extracted using the velocity information together with the momentum measurement provided by the tracking detectors. The DELPHI Barrel RICH uses liquid (C_6F_{14}) and gas (C_5F_{12}) radiators in order to cover the momentum range 1 to 20 GeV/c.

In the forward and backward regions (θ in the range $11° - 33°$ or $147° - 169°$) two additional drift chamber systems improve the tracking. Forward chamber A (FCA) consists of three pairs of wire planes, rotated by 120° with respect to each other in order to resolve internal ambiguities. Forward chamber B (FCB) consists of 12 wire planes, twice repeating the orientations of FCA. No Forward RICH information was available for the data used in this analysis.

2.1 Hadronic event selection

First the primary vertex is fitted from the measured tracks using a beam spot constraint. The beam spot position and its error are determined for each LEP fill of the 1991 data taking period. Due to beam movements in the 1992 data taking period, it is necessary to use different beam spot positions within one LEP fill. For each event the primary vertex is fitted by constraining all charged tracks to the beam spot position. This process is iterated by rejecting the tracks with the largest contribution to the overall χ^2 from the primary vertex fit until the $\chi^2/NDF < 1.5$. The precision obtained for the fitted primary vertex position perpendicular to the beam axis (xy) is dominated by the VD. From the simulation it is estimated to be 66(60) μm in $x(y)$ for the 1991 data and 50(46) μm in $x(y)$ for the 1992 data. Along the beam direction (z) the TPC dominates the precision of the primary vertex measurement, which is about 570 μm and 470 μm for the two years, respectively.

The momentum resolution of tracks at small polar angles, determined using only FCA and FCB, is improved by a constrained fit to the primary vertex if they are compatible with coming from the primary vertex.

Particles satisfying the following selection criteria are used in the analysis:

- track length > 30 cm ,
- $20^\circ \leq \theta_{track} \leq 160^\circ$,
- momentum p between 0.15 and 50.0 GeV/c ,
- relative error on $p < 100\%$,
- impact parameters $|\Delta xy| \leq 5.0$ cm and $|\Delta z| \leq 10.0$ cm .

Here the impact parameters Δxy and Δz are the distances of closest approach to the primary vertex. No impact parameter cuts are applied to tracks measured by the FCA and FCB only.

Events are accepted if:

- the total energy of charged particles $E_{ch} > 12\% \cdot \sqrt{s}$, where $\sqrt{s}$ is the centre of mass energy ,
- the charged particle multiplicity $n_{ch} \geq 5$.

These selection criteria ensure good tracking quality and agreement of DELPHI data with simulation. A sample of about 957,000 hadronic events is selected from the data taken by DELPHI in 1991 and 1992, corresponding to a selection efficiency of 96% obtained from the simulation. Due to the energy dependence of the forward-backward asymmetry, only events at the Z resonance are used for this measurement. This cut reduces the data sample to about 905,000 events. A sample of 1,118,000 JETSET 7.3 Parton Shower [3] $Z \rightarrow q\bar{q}$ events with DELPHI modifications of b and c decays and a full detector simulation [4] is used in this analysis.

3 Reconstruction of $D^{*+} \rightarrow D^\circ \pi^+$

For this analysis reconstructed D^{*+} mesons are used as a signature for $c\bar{c}$ and $b\bar{b}$ events. The D^{*+} is identified through its decay into $D^\circ \pi^+$. The charge of the low momentum pion (called slow pion π_{sl} in the following) from the D^{*+} decay is directly correlated to the charge of the primary quark. The D° is reconstructed in three different decay modes:

- $K^-\pi^+$
- $K^-\pi^+(\pi^\circ)$
- $K^-\pi^+\pi^-\pi^+$.

For all decay modes the selection of candidates is performed in a similar way. A number of charged particles corresponding to the multiplicity of the specific D° decay mode are combined, requiring the total charge to be zero. The invariant mass m_{D° of the D° candidate is calculated, assuming one of the particles to be a kaon and the others pions. The π° reconstruction is omitted for the reconstruction of the $K^-\pi^+\pi^\circ$ decay mode. This leads to a satellite peak below the nominal D° mass centre on 1.62 GeV/c^2. Candidates for the $K^-\pi^+$ and $K^-\pi^+(\pi^\circ)$ decay modes are rejected if their invariant mass is outside the initial mass interval 1.1 GeV/$c^2 \leq m_{D^\circ} \leq$ 2.65 GeV/c^2. For the $K^-\pi^+\pi^-\pi^+$ decay mode the corresponding initial mass interval is 1.7 GeV/$c^2 \leq m_{D^\circ} \leq$ 2.0 GeV/c^2.

A D^{*+} candidate is obtained by associating a low momentum pion to the reconstructed D° meson. The charge of the pion is required to be the opposite to that of the kaon from the D° meson.

For all decay modes a secondary vertex fit for the D° is performed if the mass difference Δm between the D^{*+} and the D° is below 200 MeV/c^2 and if the scaled energy, $X_E = 2 \cdot E_{D^{*+}}/\sqrt{s}$, of the D^{*+} is greater than 0.175. The aim of the secondary vertex fit

is to obtain the D° flight distance and to improve the track parameters using the vertex constraint. A D° vertex fit using the track information is performed if at least two tracks have at least one hit in the VD. Otherwise, an additional constraint is used to improve the vertex resolution, and thus the D° mass signal, since the vertex is required to be in the direction of flight of the D° candidate as determined from the momentum vector starting at the primary vertex. This approximation is also sufficient for D° from B decays, due to the low impact parameter resolution for tracks without VD information. No significant bias on the reconstructed decay length is introduced by this method. Afterwards the slow pion from the D^{*+} decay is constrained to the D° vertex, which is a good approximation for the D^{*+} decay vertex because of the small transverse momentum of the slow pion to the direction of flight of the D°.

The distance between the primary and the D° vertex is calculated in the xy plane and projected on the D° direction of flight to obtain the decay length ΔL. A vertex combination is accepted if ΔL is within -0.25 cm and 2 cm for the $K^-\pi^+$ and $K^-\pi^+(\pi^\circ)$ decay mode. For the $K^-\pi^+\pi^-\pi^+$ decay mode the interval -0.025 cm $\leq \Delta L \leq 2$ cm is used to reduce the higher combinatorial background. A further reduction of background is achieved by rejecting track combinations with large impact parameters Δxy and Δz with respect to the fitted D° vertex. Therefore the quantity:

$$\chi^2_\delta = (\Delta xy\ \Delta z) \begin{pmatrix} \sigma^2_{\Delta xy} & cov(\Delta xy, \Delta z) \\ cov(\Delta xy, \Delta z) & \sigma^2_{\Delta z} \end{pmatrix}^{-1} \begin{pmatrix} \Delta xy \\ \Delta z \end{pmatrix}$$

is defined, taking the errors of the impact parameters into account. A vertex combination is rejected if the χ^2_δ of a track from the D° candidate is larger than 25 for the two and three body decay modes or 50 for the $K^-\pi^+\pi^-\pi^+$ decay mode. For the slow pion, which is constrained to the D° vertex, a value χ^2_δ less than 100 is demanded. After this the vertex information is used to improve the track parameters and thus the invariant mass resolution.

D° decay mode	cut on helicity angle $\cos\theta_H$
$D^\circ \to K^-\pi^+,\ K^-\pi^+(\pi^\circ)$	$\lvert\cos\theta_H\rvert\ <\ 1/3 \cdot \ln(2 \cdot X_E - 0.2) + 1$
$D^\circ \to K^-\pi^+\pi^-\pi^+$	$\lvert\cos\theta_H\rvert\ <\ 1/2 \cdot \ln(2 \cdot X_E - 0.2) + 1$

Table 1: Helicity angle cuts.

Cuts on the helicity angle distribution (see table 1) are used to achieve a further significant reduction of the combinatorial background. The helicity angle $\cos\theta_H$ is defined as the angle of the kaon in the D° rest frame with respect to the D° direction of flight. D° decays are isotropic in $\cos\theta_H$, whereas the background is extremely peaked at $\cos\theta_H = \pm 1$. For the $K^-\pi^+\pi^-\pi^+$ decay mode similar information is obtained from the sphericity axis of the four particles in the D° system. Due to the energy spectrum of charged particles in hadronic Z events the combinatorial background is concentrated at small $X_E(D^{*+})$. Therefore X_E dependent cuts on the helicity angle are used to allow for higher background contributions at small D^{*+} energies. The X_E of the D^{*+} combination is required to be larger than 0.2.

The mass bands to select the different D° decay modes and the cuts on the mass difference are listed in table 2. The mass difference and D° mass distributions for the three decay modes are shown in figures 1 and 2, respectively. The histograms show the

D° decay mode	ΔL for D° [cm]	max. χ^2_δ of impact parameter		D° mass interval [GeV/c^2]	max. Δm [GeV/c^2]
		D° tracks	π_{sl} track		
$K^-\pi^+$	-0.25 to 2.0	25	100	1.79 to 1.94	0.1525
$K^-\pi^+\pi^-\pi^+$	-0.025 to 2.0	50	100	1.81 to 1.92	0.1525
$K^-\pi^+(\pi^\circ)$	-0.25 to 2.0	25	100	1.35 to 1.75	0.1700

Table 2: Cuts for the D^{*+} selection.

simulated distributions normalized to the data samples. The contributions of signal and background are adjusted to compensate for different D^{*+} rates in data and simulation.

4 Particle identification

A reduction of the combinatorial background has been obtained using the particle identification provided by the barrel RICH and the dE/dx measurement of the TPC. Due to the large number of pions in the hadronic final state, combinations in which a pion is assigned as a kaon candidate provide the main contribution to the background. To optimize the efficiency of the D^{*+} signal a pion veto, rather than a kaon identification, has been introduced.

496,000 (235,000) events are available with gas (liquid) radiator information in the DELPHI data of 1991 and 1992. The simulation was tuned to reproduce the identification efficiency present in the data. The relevant momentum range for kaons from D^{*+} corresponds mainly to the sensitive range of the gas radiator. Due to the Cherenkov thresholds for the different particles, a positive identification is not possible over the whole momentum range. Above 3 GeV/c, pions radiate light in the gas radiator, while the threshold for kaons is 8 GeV/c. Separation between kaons and pions is possible up to 20 GeV/c, where the expected Cherenkov angles for both hypotheses become maximal. For kaon candidates below 3 GeV/c the liquid radiator information is used.

The different thresholds are taken into account in the calculation of the global probabilities $P^{RICH}_{e,\mu,\pi,K,p}$ from the measured single photon distributions using a maximum likelihood technique [5]. For a pion veto it is sufficient to calculate only the probabilities for pions, kaons and protons, because in the relevant momentum range the Cherenkov angle for photons from light particles (pions, muons and electrons) is almost maximal and they can all be treated as pions. A momentum independent two class separation is obtained by normalizing the probabilities for kaon and proton to the sum for kaon, proton and pion:

$$tag|_{RICH} \;=\; \frac{P_K^{RICH} + P_P^{RICH}}{P_K^{RICH} + P_P^{RICH} + P_\pi^{RICH}} \; .$$

The pion veto identification for kaons and pions taken from the decay $D^{*+} \rightarrow (K^-\pi^+)\pi^+$ is shown in figure 3 (a+b). Due to the good separation quality the cut on the $tag|_{RICH}$ distribution of the kaon candidates is fixed for the whole D^{*+} energy range and for all analysed decay modes:

$$tag|_{RICH} \;>\; 0.25 \; .$$

At least 30 independent TPC measurements per track are required to obtain the dE/dx information. This condition is fulfilled for 63% of the tracks. A calibration is performed

to obtain a standard Gaussian distribution around the correct particle expectation for the measured dE/dx, normalized to its error σ. The expectation values $dE/dx|_{K/\pi}$ for kaons and pions are distinguished for momentum p greater than 1.5 GeV/c. In this region an average separation of 1.4 standard deviations between kaons and pions is provided by the dE/dx measurement. No dE/dx information is used for particles below 1.5 GeV/c. The probability density to measure a dE/dx value for a pion or a kaon is given by a Gaussian distribution around the pion or kaon expectation value:

$$P_{K/\pi}^{TPC} \;=\; e^{-\frac{1}{2}\left(\frac{dE/dx - dE/dx|_{K/\pi}}{\sigma}\right)^2} \;.$$

In general, light particles (π, e, μ) have a higher pion probability P_π^{TPC} rather than kaon probability P_K^{TPC}, while heavy particles (K, p) have a higher kaon than pion probability. For this reason, the two class separation needed for a veto, is obtained by renormalizing the kaon probability density:

$$tag|_{TPC} \;=\; \frac{P_K^{TPC}}{P_K^{TPC} + P_\pi^{TPC}} \;.$$

The K/π separation is shown in figure 3 (c+d) for a pion and an enriched kaon sample from the decay $D^{*+} \to (K^-\pi^+)\pi^+$, respectively. The cut on $tag|_{TPC}$ distribution is X_E dependent to account for the different energy spectra of D^{*+} signal and background. For all analysed decay modes, the cut used for the kaon candidates as a veto against pions is:

$$tag|_{TPC} \;>\; 0.1 - 0.1 \cdot \ln(X_E - 0.1) \;.$$

5 Measurement of $A_{FB}^{c\bar{c}}$ and $A_{FB}^{b\bar{b}}$

For a measurement of $A_{FB}^{c\bar{c}}$ and $A_{FB}^{b\bar{b}}$ from the $\cos\theta$ distribution of D^{*+} it is necessary to separate D^{*+} from $c\bar{c}$ and $b\bar{b}$ events and the combinatorial background. Since the c and b asymmetries are expected to be of comparable size and to have the same relative sign, the statistical precision of the measurement is limited by the negative correlation between both asymmetries. In this analysis, a good separation, giving a relatively small correlation, is obtained by using the scaled energy distribution X_E of the D^{*+} candidates and the D° decay distance to distinguish between the different classes. The hadronization of primary c quarks leads to high energy D^{*+} mesons, whereas b quarks fragment into b hadrons, which then decay into D^{*+} mesons with a softer energy spectrum. On the other hand, a larger D° decay distance is expected for b events due to the long lifetime of B hadrons, compared with the short lifetime of D° mesons. This difference was used in [6] to measure the production of D^{*+} mesons from c and b events separately. The combinatorial background is concentrated at low X_E and small decay distances. It is estimated from the sidebands in the mass difference distribution. Due to the different relative acceptance of D^{*+} mesons and background at small and large polar angles, the fit method has to account for the $|\cos\theta|$ dependence of the different classes.

For the asymmetry measurement, partially reconstructed D^{*+} mesons $(\pi_{sl} + X)$ and reflections from other decay modes (see figure 1) have to be considered as signal to avoid charge correlations in the background. The contributions from reflections, where some particles from the D° decay are assigned the wrong mass or are missing, and true $K^-\pi^+(\pi^\circ)$ decays are treated as one class, because of the similar shape of the signals and the charge correlation with the primary quark, which is given by the slow pion from the

D^{*+} decay. This leads to a significant increase of the sample for the $K^-\pi^+(\pi^\circ)$ decay mode, where about 46% of the signal originates from reflections. The rate of partially reconstructed D^{*+} mesons, where a slow pion from a D^{*+} decay is combined with a fake D° candidate which includes some particles not actually from the D° decay, depends on the branching ratio $D^{*+} \to D^\circ\pi^+$, the D^{*+} production rate and the efficiency in the relevant mass difference interval. The contribution of partially reconstructed D^{*+} decays to the signal is taken from the simulation and contributes to the systematic error.

To avoid double counting of events, only the D^{*+} candidate with the D° mass closest to the nominal mass is retained. The D^{*+} candidate with the smallest mass difference is selected in case of more than one combination with the same D° candidate. Due to this method no artificial peak is introduced in the mass difference distribution, as shown in figure 1. For the $K^-\pi^+(\pi^\circ)$ decay mode, the central value of 1.62 GeV/c^2 for the satellite peak is used instead of the D° mass. Events entering the $K^-\pi^+$ decay mode are removed from the $K^-\pi^+\pi^-\pi^+$ distribution and events from both decay modes are then removed from the $K^-\pi^+(\pi^\circ)$ distribution. The number of reconstructed D^{*+} decays given in table 3 is obtained from the fit to the mass spectra. The prediction from simulation for reflections in the D^{*+} signals and the rates of partially reconstructed D^{*+} mesons in the combinatorial background are listed in the third and fourth column, respectively. A total sample of 4757 reconstructed D^{*+} decays is used for the asymmetry measurement.

D° decay mode	$D^{*+} \to D^\circ\pi^+$ events	rate of reflections in D^{*+} signal	rate of $\pi_{sl} + X$ in background
$K^-\pi^+$	1167 $\pm$ 46	4%	11%
$K^-\pi^+\pi^-\pi^+$	899 $\pm$ 79	8%	18%
$K^-\pi^+(\pi^\circ)$	2691 $\pm$ 143	46%	10%

Table 3: D^{*+} sample used for the measurement.

5.1 The unbinned maximum likelihood fit

The determination of the asymmetries is achieved by an unbinned maximum likelihood fit (similar to the one used in [7]) to the D^{*+} samples using the mass difference, scaled energy, polar angle and D° decay distance distributions. Figures 4-6 compare the measured distributions for the different decay modes with the predictions of the simulation, split into charm, bottom and background events. The simulated prediction is normalized to the data to reproduce the signal to background ratio. Therefore a factor $R_{S/B}$ is introduced for each decay mode, which compensates for different D^{*+} rates in data and simulation. After this correction a good agreement is found in all distributions. The shape of the background distribution, as obtained from the sidebands, is well reproduced by the Monte Carlo.

For each decay mode a distance is defined in a four dimensional space:

$$\mathcal{D}_{1,2} = \left\{ \frac{(\Delta m_1 - \Delta m_2)^2}{\mathrm{scale}^2_{\Delta \mathrm{m}}} + \frac{(X_{E,1} - X_{E,2})^2}{\mathrm{scale}^2_{\mathrm{X_E}}} + \frac{(|\cos\theta_1| - |\cos\theta_2|)^2}{\mathrm{scale}^2_{|\cos\theta|}} + \frac{(\Delta L_{tr,1} - \Delta L_{tr,2})^2}{\mathrm{scale}^2_{\Delta \mathrm{L_{tr}}}} \right\}^{\frac{1}{2}} .$$

The transformation $\Delta L_{tr} = \mathrm{sign}\left(\frac{\Delta \mathrm{L}}{\mathrm{cm}}\right) \cdot \left(1 - \mathrm{e}^{-2\frac{|\Delta \mathrm{L}|}{\mathrm{cm}}}\right)$ of the D° decay distance and the scales (see table 4) for each distribution are used to obtain an approximately constant

density in the variable space of simulated events around each data point. To calculate the probabilities that a D^{*+} candidate belongs to a given class, the N_{MC} simulated events with the smallest distance $\mathcal{D}_{1,2}$ to the data event are collected. For this analysis $N_{MC} = 50$ is chosen for the $K^-\pi^+$ decay mode and $N_{MC} = 100$ for the $K^-\pi^+\pi^-\pi^+$ and $K^-\pi^+\pi^0$ decay modes, which is optimized to the available statistics. The probability for each data event to be a charm, bottom or background event is given by:

$$P_k(\Delta m, X_E, |\cos\theta|, \Delta L_{tr}) = \frac{W_k}{\sum\limits_l W_l} \ .$$

Here W_k is the weighted number of simulated events from class k, while k stands for charm, bottom or background, respectively. The weight for charm and bottom events is given by $R_{S/B}$ to compensate for D^{*+} production rates being slightly different in data and simulation. For background events the weight is one. The asymmetry for a fixed polar angle then determines the contribution to the log likelihood according to the different classes:

$$F_k(\theta, A_k) = \frac{1}{2}\left(1 + \frac{8}{3}A_k\frac{\cos\theta}{1+\cos^2\theta}\right) \ ,$$

where A_k is the integrated asymmetry of class k, which in case of the b asymmetry includes a correction for $B - \bar{B}$ oscillation effects (see section 5.2). Then the negative logarithm of the likelihood function to be minimized is obtained combining the information from all decay modes:

$$\mathcal{L} = -\sum_{j=1}^{N_{Data}} \ln\left\{\sum_{k=1}^{3} P_{k,j}F_k(\theta_j, A_k)\right\} \ .$$

D° decay mode	N_{MC}	$\text{scale}_{\Delta\text{m}}$	$\text{scale}_{\lvert\cos\theta\rvert}$	$\text{scale}_{\text{X}_\text{E}}$	$\text{scale}_{\Delta\text{L}_\text{tr}}$	$R_{S/B}$
$K^-\pi^+$	50	1.0 MeV/c^2	0.2	0.1	0.15	91 %
$K^-\pi^+\pi^-\pi^+$	100	1.0 MeV/c^2	0.2	0.1	0.15	102 %
$K^-\pi^+(\pi^\circ)$	100	2.0 MeV/c^2	0.2	0.1	0.15	105 %

Table 4: Scales and normalization factors used in the calculation of the probabilities.

5.2 $B - \bar{B}$ oscillation effects

To obtain the b quark asymmetry, the effective D^{*+} asymmetry observed in bottom events has to be corrected for mixing of neutral B mesons:

$$A_{FB}^{b\bar{b},mix} = (1 - 2\chi)\cdot A_{FB}^{b\bar{b}} \ .$$

Since the D° decay length is used to separate charm and bottom events, the time dependence of the $B_d^\circ - \bar{B}_d^\circ$ oscillation effect, measured in [1], needs to be taken into account. Due to the incomplete momentum reconstruction of the B_d°, the proper decay time cannot be calculated. Using the average Lorentz boost $\gamma\beta$ of B_d° mesons, the dependence of the $B_d^\circ - \bar{B}_d^\circ$ oscillation can be parameterized as a function of the sum of the B_d° and D° decay lengths ΔL:

$$\chi_d(\Delta L) = \frac{1}{2}\left\{1 - \cos\left(\Delta m_d \cdot \gamma\beta\Delta L \cdot a_1\right)\cdot(1 - a_2\Delta L)\right\} \ . \qquad (3)$$

The world average value $\Delta m_d = 0.500 \pm 0.033\,\mathrm{ps}^{-1}$ [8] is taken for the oscillation frequency. The correction factors $a_1 = 0.7\frac{\mathrm{ps}}{\mathrm{cm}}$ and $a_2 = \frac{0.14}{\mathrm{cm}}$ are obtained from Monte Carlo simulation, taking also vertex resolution effects into account. A lifetime independent scheme is applied to correct for $B_s^\circ - \bar{B}_s^\circ$ oscillation, using χ_s between 0.4 and 0.5 as expected in the Standard Model.

The size of the correction for the mixing effects depends on the relative rate of D^{*+} mesons from the different B mesons. The individual contributions to the D^{*+} production in B decays are obtained from the JETSET 7.3 model with DELPHI modifications for b and c decays. The probabilities to form a B meson from a b quark are set to $0.39 \pm 0.02(B_s^\circ) \pm 0.03$(baryons) for B_d° and B_u^+ and to 0.12 ± 0.04 and 0.10 ± 0.06 for B_s° and baryons, respectively. The vector to vector plus pseudoscalar ratio $\frac{V}{V+P}$ for direct produced $L = 0$ charmed mesons D and D^* is assumed to be 0.75. The production rate of p-wave mesons in B decays is adjusted to 24% of the total D meson production, leading to a ratio of D^* to D mesons in agreement with recent measurements [6,9]. The relative rates of the different $L = 1$ states are determined by their spin weight.

As listed in table 5, the main contribution to the D^{*+} production is given by B_d° decays, while the production from B_u^+ and B_s° is suppressed. The inclusive branching ratio $B_{d,u} \to D^{*+} + X$ is in agreement with the measurement of $(23 \pm 4)\%$ [10]. Contributions from decays of B_c^+ mesons and gluon splitting are of minor importance. Another process, leading to an observed b asymmetry with negative sign, is the decay $\bar{b} \to W^+ \to c \to D^{*+}$. Here the relative contributions to the asymmetry are given by the production probabilities for the different b hadrons and have to be corrected for mixing. The rate for this process is expected to be less than 3% of the total D^{*+} production in B decays.

contribution	relative rate	asymmetry
$\bar{B}_d^\circ \to D^{*+} + X$	68%	$(1 - 2\chi_d(\Delta L)) \cdot A_{FB}^{b\bar{b}}$
$B_u^- \to D^{*+} + X$	20%	$A_{FB}^{b\bar{b}}$
$\bar{B}_s^\circ \to D^{*+} + X$	4%	$(1 - 2\chi_s) \cdot A_{FB}^{b\bar{b}}$
b − baryon $\to$ D^{*+} + X	4%	$A_{FB}^{b\bar{b}}$
$\bar{b} \to W^+ \to c \to D^{*+}$	3%	see text
gluon splitting, B_c, ...	1%	~ 0

Table 5: Relative contributions to the D^* sample from b events, as obtained from the simulation.

5.3 The fit result

Taking into account the lifetime evolution of the $B_d^\circ - \bar{B}_d^\circ$ oscillation, a three parameter fit of the charm, bottom and background asymmetry to the combined D^{*+} sample yields:

$$A_{FB}^{c\bar{c}} = 0.077 \pm 0.029\,(\mathrm{stat}) \quad \text{and} \quad \mathrm{A_{FB}^{b\bar{b}}} = 0.059 \pm 0.062\,(\mathrm{stat})\ ,$$

with a correlation coefficient of -0.38. The background asymmetry A_{FB}^{back} is found to be $-0.002 \pm 0.009\,(\mathrm{stat})$. Furthermore, no significant asymmetry is observed in the background of the individual decay modes. In figure 7 (a+b) the comparison of the data to the fit result for the forward-backward asymmetry of D^{*+} events is shown as a function of X_E and $\Delta L_{tr}(D^\circ)$. The differential asymmetry $A_{diff} = \frac{8}{3} \cdot A_{FB} \cdot \frac{\cos\theta}{1+\cos^2\theta}$ is shown in figure 7 (c). The results of the fits to the individual decay modes are listed in table 6.

D° decay mode	$A_{FB}^{c\bar{c}}$	$A_{FB}^{b\bar{b}}$	A_{FB}^{back}
$K^-\pi^+$	0.056 $\pm$ 0.054	0.110 $\pm$ 0.098	0.004 $\pm$ 0.043
$K^-\pi^+\pi^-\pi^+$	0.075 $\pm$ 0.060	0.090 $\pm$ 0.136	-0.008 $\pm$ 0.018
$K^-\pi^+(\pi^\circ)$	0.092 $\pm$ 0.043	-0.004 $\pm$ 0.101	0.002 $\pm$ 0.012

Table 6: Fit results of the three parameter fit to the individual decay modes.

In an attempt to reduce the error on the charm asymmetry, a two parameter fit of the constrained charm asymmetry $A_{FB}^{c,const}$ and A_{FB}^{back} is performed. From the DELPHI measurements $A_{FB}^{b\bar{b}} = 0.107 \pm 0.011$ and $A_{FB}^{c\bar{c}} = 0.083 \pm 0.027$ [11] using prompt leptons and lifetime tag, one obtains $A_{FB}^{b,const} = 0.102 + 0.059 \cdot A_{FB}^{c,const}$ for the constrained bottom asymmetry, taking the +15% correlation between the charm and bottom asymmetry for this measurement into account. The effective b asymmetry is calculated correcting $A_{FB}^{b,const}$ for oscillation of neutral B mesons. A two parameter fit to the data yields for the constrained charm asymmetry:

$$A_{FB}^{c,const} = 0.068 \pm 0.027\,(\text{stat})\ .$$

Again the asymmetry of the background $A_{FB}^{back} = -0.004 \pm 0.009$ is compatible with zero. These results are measured at an average centre of mass energy of $\sqrt{s} = 91.27 \pm 0.02$ GeV.

6 Systematic errors

Differences between the signal and background efficiency as a function of $\cos\theta$ are considered in the calculation of the probabilities from the simulation. Since the asymmetry enters in the likelihood as a function of $\cos\theta$, the sensitivity to efficiency variations is small.

For all decay modes the relative normalization $R_{S/B}$ is obtained from a fit of the simulated D^{*+} signal and background to the data. A variation of $\pm$15% is included in the systematic error, not only to account for the error of the fitted $R_{S/B}$, but also for uncertainties in the agreement of the shape of the mass difference signals in data and simulation.

The simulation is adjusted in order to reproduce the production rates and the average energy of D^{*+} mesons in charm and bottom events as measured by the LEP experiments [6,9,12]. The systematic errors are derived taking differences between the energy spectrum in data and simulation into account. A variation of $\pm$15% of the ratio of charm to bottom events is considered as the systematic error. The error due to the uncertainty of the average D^{*+} energy is considered by varying the average energy fraction carried by b hadrons between 0.67 and 0.72 and the average D^{*+} energy in c events between 0.48 and 0.52.

In the simulation a B lifetime $\tau_B = 1.6$ ps is used, which is in good agreement with the world average [13]. A variation between 1.35 and 1.85 ps is considered in the determination of the systematic error to allow for the error on τ_B and for differences in the shape of the ΔL distribution in data and simulation.

The systematic error on the mixing correction depends on the uncertainty of the effective reconstructed B lifetime, which is obtained from the D° decay length, and on the error of oscillation frequency, where the measured oscillation frequency

$\Delta m_d = 0.500 \pm 0.033\,\mathrm{ps}^{-1}$ [8] is used for the calculation. The errors assigned to the correction factors a_1 and a_2 in equation 3 include resolution effects on the D° vertex.

The influence of the mixing effect on the observed b asymmetry depends on the relative contributions to the b sample. The systematic error is determined by a variation of the relative rate of D^{*+} from B_d° between 55 % and 85 % by changing the decay properties inside the model. The influence of the uncertainty on χ_s is found to be negligible.

The systematic error due to the contribution of partially reconstructed D^{*+} decays is estimated by a 30% variation of the prediction of the simulation. This includes uncertainties on the efficiency to reconstruct such $\pi_{sl} + X$ combinations as well as on the total rate of $D^{*+} \to D^\circ \pi^+$ decays in hadronic Z events. The systematic error also accounts for the uncertainty of the mixing correction for partially reconstructed D^{*+} decays. Since the slow pion is combined with a fake D° candidate, the decay length distribution and thus the B_d° oscillation correction has to be modified for $\pi_{sl} + X$ events. The effect is corrected using the simulation and a variation of 100 % of the correction is included as the systematic error.

From the distributions of fit results of 1000 simulated data sets the statistical error due to the finite simulated sample is derived subtracting the statistical errors of the data sample quadratically from the width of the distributions. A systematic error is introduced due to the limited number of simulated events N_{MC} used to determine the probabilities in the likelihood function. The effect is estimated from the shift of the distributions of fit results relative to the simulated asymmetries of 0.07 and 0.10 for c and b quarks, respectively. The stability of the fit is tested by an uncorrelated 30% variation of N_{MC} and of the scales entering the distance function $\mathcal{D}_{1,2}$.

systematic error source	$A_{FB}^{c\bar{c}}$	$A_{FB}^{b\bar{b}}$	$A_{FB}^{c,const}$
normalization $\frac{signal}{background}$	∓ 0.003	∓ 0.002	∓ 0.003
$(\gamma_c \cdot P_{c\to D^*})/(\gamma_b \cdot P_{b\to D^*})$	∓ 0.002	± 0.001	∓ 0.001
$\langle x_c \rangle$	± 0.001	± 0.002	± 0.001
$\langle x_b \rangle$	± 0.001	∓ 0.001	∓ 0.001
τ_b	± 0.002	∓ 0.004	∓ 0.001
B_d° oscillation	∓ 0.003	± 0.012	± 0.002
contributions to b sample	∓ 0.002	± 0.005	± 0.002
rate of $\pi_{sl} + X$	∓ 0.006	± 0.009	∓ 0.005
fit method	± 0.006	± 0.015	± 0.005
MC statistics	± 0.005	∓ 0.009	± 0.005
detector effects	± 0.004	± 0.002	± 0.004
D^* instead of quark direction	± 0.001	± 0.001	± 0.001
$\Delta A_{FB}^{b\bar{b}}$ for constraint fit	–	–	∓ 0.003
total	0.012	0.024	0.011

Table 7: Contributions to the systematic errors on the measured asymmetries. The estimated correlation coefficient between the systematic errors of $A_{FB}^{c\bar{c}}$ and $A_{FB}^{b\bar{b}}$ in the combined fit is -0.22.

A shift in the central value or in the width of the reconstructed invariant mass distribution for D° mesons relative to $\bar{D}^\circ$ mesons can also affect the asymmetry measurement if it is different in the two detector hemispheres. An upper limit for the systematic error

on the charm asymmetry is ± 0.004 and ± 0.002 for the bottom asymmetry, taking the energy dependence of the width of the reconstructed D° mass distribution into account.

The error of the asymmetry due to the determination of the primary quark direction by the D^{*+} direction is derived from the predictions of different models.

The error of the constrained fit of the charm asymmetry, using the DELPHI b asymmetry measurement from prompt leptons and lifetime tag, is obtained from the errors quoted in [11].

The contributions to the systematic errors for the combined fit of the charm and bottom asymmetries and for the constrained fit are listed in table 7. The relative sign of the systematic error indicates the direction in which the results change for a particular error source. The estimated correlation coefficient between the systematic errors of $A_{FB}^{c\bar{c}}$ and $A_{FB}^{b\bar{b}}$ in the combined fit is -0.22.

7 The effective electroweak mixing angle

To obtain an effective electroweak mixing angle from the measured charm quark forward-backward asymmetry a few corrections have to be applied to obtain the bare asymmetry $A_{FB}^{\circ,c}$.

The asymmetry is measured at $\sqrt{s} = 91.27 \pm 0.02$ GeV and must be corrected to $\sqrt{s} = M_Z$. The slope of the asymmetry around M_Z depends only on the axial vector coupling and the charge of the final state fermion. It is thus independent of the pole asymmetry itself. The correction due to the energy shift and the QED correction for initial state radiation have been calculated using ZFITTER [14].

The QCD correction to the forward-backward asymmetries using the charm quark direction is calculated in [15] to be:

$$A_{FB}^{QCD} = A_{FB}^{noQCD} \cdot \left(1 - c_1 \frac{\alpha_s(M_Z)}{\pi} + c_2 \left(\frac{\alpha_s(M_Z)}{\pi}\right)^2\right) .$$

For charm quarks the value c_1 is given by $c_1 \simeq 0.95 - 0.93$ for $m_c = 1.1$ to 1.7 GeV/c^2, while c_2 is -4.4 ± 0.4. Here $\alpha_s(M_Z) = 0.123 \pm 0.006$ [16] is used as the central value for the calculation. The QCD corrections are modified due to implicit cuts on events with hard gluons. For this reason an error of $\pm 25\%$ and $\pm 100\%$ is assigned to c_1 and c_2, respectively. In the likelihood fit charm production from gluon splitting in $e^+e^- \to f\bar{f}$ events, with $f \neq c$, is taken from the Monte Carlo and does not contribute to the charm class. Therefore no additional correction has to be applied.

source	ΔA_{FB}
$\sqrt{s} = M_Z$	-0.0034
QED corrections	$+0.0104$
QCD corrections	$+0.0031 \pm 0.0009$
$\gamma, \gamma Z$	-0.0008
total	$+0.0093 \pm 0.0009$

Table 8: Corrections applied to the charm asymmetry.

The small corrections for γ exchange and γZ interference have again been calculated using ZFITTER. The corrections summarized in table 8 are to be understood as

$A_{FB}^{\circ,c} = A_{FB}^{c\bar{c}} + \sum \Delta A_{FB}$. From the fit result $A_{FB}^{c,const} = 0.068 \pm 0.027\,(\text{stat}) \pm 0.011\,(\text{sys})$ the bare asymmetry $A_{FB}^{\circ,c}$ is calculated to be:

$$A_{FB}^{\circ,c} = 0.077 \pm 0.027\,(\text{stat}) \pm 0.012\,(\text{sys}) \ .$$

From this bare asymmetry the effective electroweak mixing angle $\sin^2\theta_{eff}^{lept}$ is calculated using equations 1 and 2:

$$\sin^2\theta_{eff}^{lept} = 0.2307 \pm 0.0062\,(\text{stat}) \pm 0.0026\,(\text{sys}) \ .$$

8 Conclusion

The forward-backward asymmetries for charm and bottom quarks at the Z pole are measured simultaneously from the polar angle, mass difference, scaled energy and D° decay distance distributions of 4757 D^{*+} mesons using a unbinned maximum likelihood fit. Taking the lifetime evolution of the $B_d^\circ - \bar{B}_d^\circ$ oscillation into account, the fit yields:

$$A_{FB}^{c\bar{c}} = 0.077 \pm 0.029\,(\text{stat}) \pm 0.012\,(\text{sys}) \quad \text{and} \quad \mathrm{A_{FB}^{b\bar{b}}} = 0.059 \pm 0.062\,(\text{stat}) \pm 0.024\,(\text{sys}) \ .$$

The total correlation coefficient between $A_{FB}^{c\bar{c}}$ and $A_{FB}^{b\bar{b}}$ is -0.36. Constraining the b asymmetry to the value measured by DELPHI using prompt leptons and lifetime tag [11], the charm asymmetry is determined to be:

$$A_{FB}^{c,const} = 0.068 \pm 0.027\,(\text{stat}) \pm 0.011\,(\text{sys}) \ .$$

Good agreement with recent results from other experiments using the same method [9,12] and using inclusive leptons [11,17] is found. The charm asymmetry $A_{FB}^{c,const}$ corresponds to the bare asymmetry $A_{FB}^{\circ,c} = 0.077 \pm 0.027\,(\text{stat}) \pm 0.012\,(\text{sys})$, from which the effective electroweak mixing angle $\sin^2\theta_{eff}^{lept}$ is calculated:

$$\sin^2\theta_{eff}^{lept} = 0.2307 \pm 0.0062\,(\text{stat}) \pm 0.0026\,(\text{sys}) \ .$$

This result is in good agreement with the effective electroweak mixing angle derived from several measurements at LEP and SLC [18].

Acknowledgement

We are greatly indebted to our technical collaborators and to the funding agencies for their support in building and operating the DELPHI detector, and to the members of the CERN-SL Division for the excellent performance of the LEP collider.

References

[1] ALEPH Collaboration, D.Buskulic et al., Phys. Lett.**B313** (1993) 498
DELPHI Collaboration, P.Abreu et al., Phys. Lett. **B338** (1994) 409
OPAL Collaboration, R.Akers et al., Phys. Lett. **B327** (1994) 411

[2] DELPHI Collaboration, P.Aarnio et al., Nucl. Inst. and Meth. **A303** (1991) 233

[3] T. Sjöstrand, *JETSET 7.3 Manual*, CERN TH/92-6488, Geneva 1992

[4] DELPHI Collaboration, *DELSIM Reference Manual*,
DELPHI Note 87-98, Geneva 1989

[5] P. Baillon, Nucl. Inst. and Meth. **A238** (1985) 341

[6] DELPHI Collaboration, P.Abreu et al., Z. Phys. **C59** (1993) 533

[7] DELPHI Collaboration, P.Abreu et al., Phys. Lett. **B276** (1992) 536

[8] R. Forty, *CP violation and $B\bar{B}$ mixing*, talk given at the 27th International Conference on High Energy Physics, Glasgow, 1994

[9] ALEPH Collaboration, D Buskulic et al., Z. Phys. **C62** (1994) 1

[10] Particle Data Group, Phys. Rev. **D50** (1994) 1173

[11] DELPHI Collaboration, *Measurement of the Forward-Backward Asymmetry of $e^+e^- \to Z^0 \to b\bar{b}$ using prompt leptons and micro-vertex tag*,
CERN PPE/94-161, Geneva 1994, to be published in Z. Phys. C

[12] OPAL Collaboration, R.Akers et al., Z. Phys. **C60** (1993) 601

[13] P. Roudeau, *Heavy Flavours - strong interactions*, talk given at the 27th International Conference on High Energy Physics, Glasgow, 1994

[14] D.Bardin et al., *ZFITTER: An Analytical Program for Fermion Pair Production in e^+e^- Annihilation*, CERN-TH. 6443/92, Geneva 1992

[15] G.Altarelli, B.Lampe, Nucl. Phys. **B391** (1993) 3

[16] DELPHI Collaboration, P.Abreu et al., Z. Phys. **C59** (1993) 21

[17] ALEPH Collaboration, D.Buskulic et al., Z. Phys. **C62** (1994) 179
L3 Collaboration, O.Adriani et al., Phys. Lett. **B292** (1992) 454
OPAL Collaboration, R.Akers at al., Z. Phys. **C60** (1993) 199

[18] D.Schaile, *Precision Tests of the Electroweak Interactions*, talk given at the 27th International Conference on High Energy Physics, Glasgow, 1994

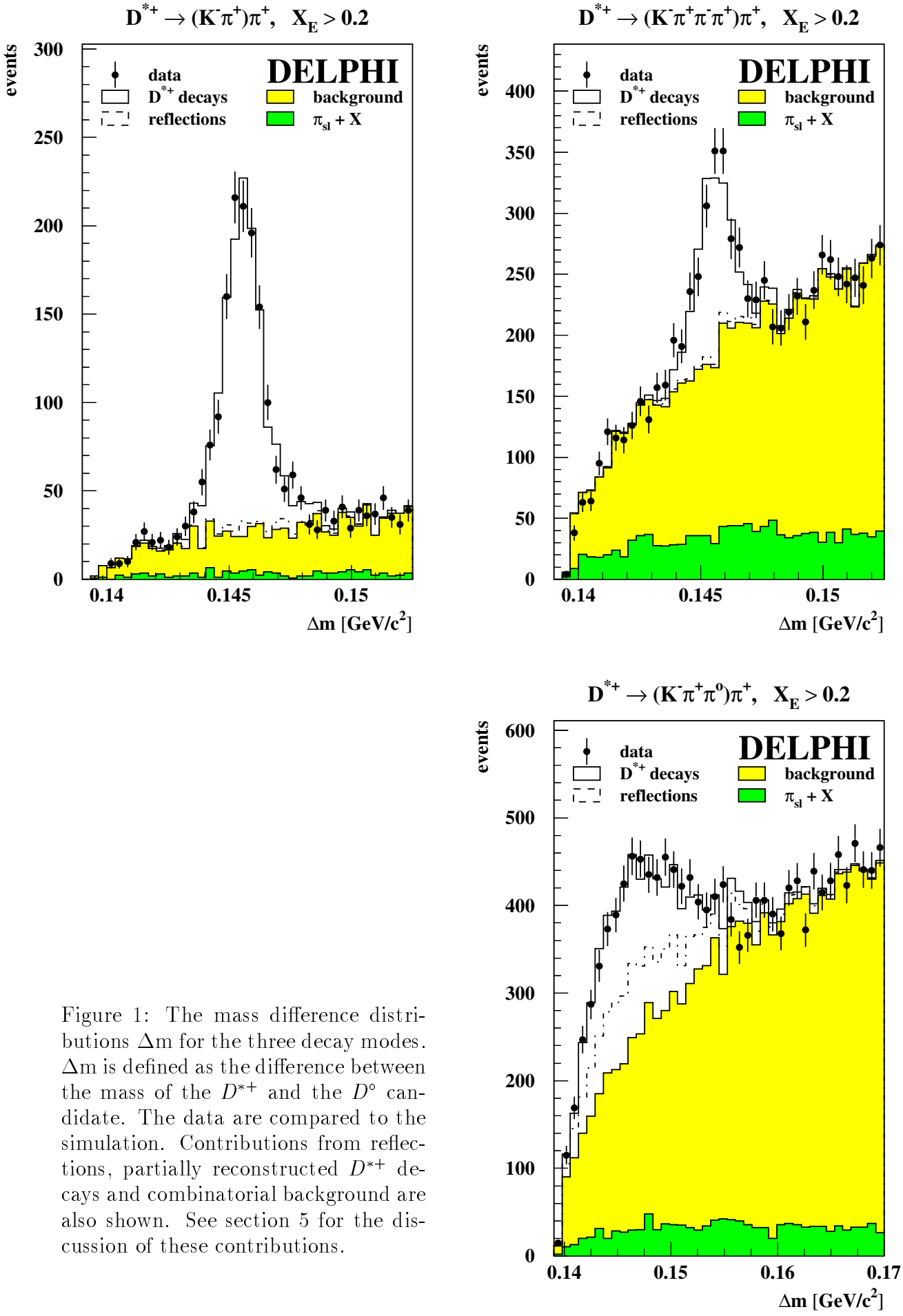

Figure 1: The mass difference distributions Δm for the three decay modes. Δm is defined as the difference between the mass of the D^{*+} and the D^0 candidate. The data are compared to the simulation. Contributions from reflections, partially reconstructed D^{*+} decays and combinatorial background are also shown. See section 5 for the discussion of these contributions.

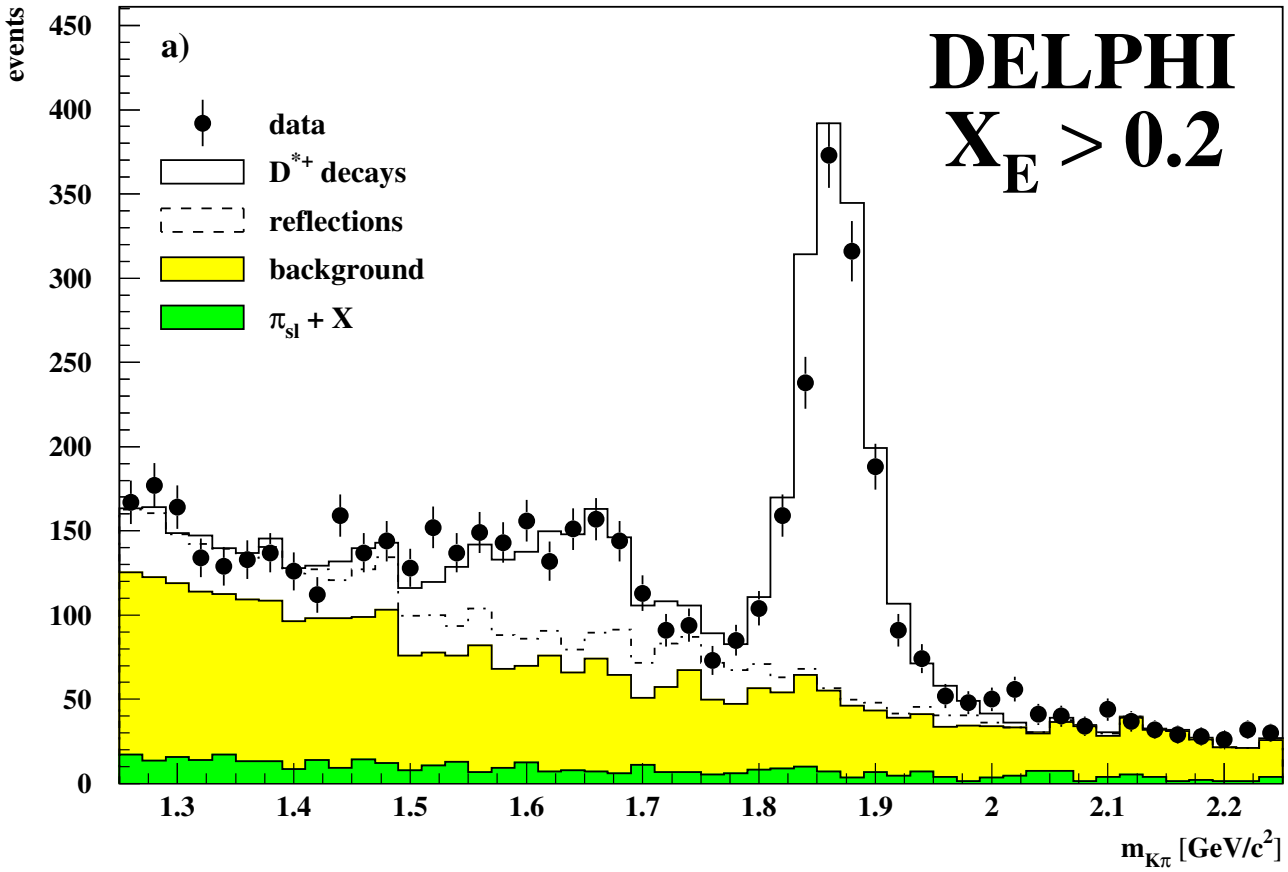

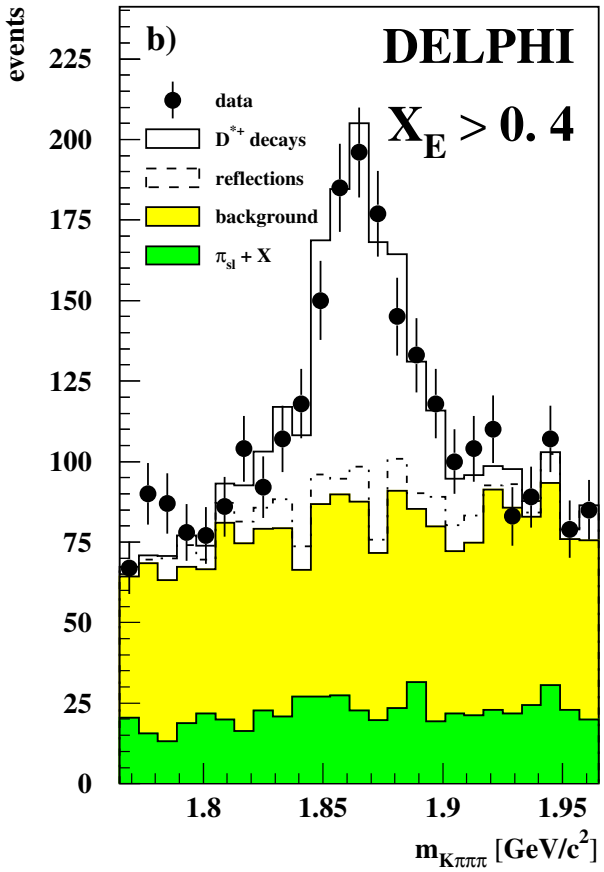

Figure 2: (a) The $K^-\pi^+$ and (b) $K^-\pi^+\pi^-\pi^+$ mass distributions from D^{*+} candidates with a mass difference Δm in the interval between 0.1435 GeV/c^2 and 0.1475 GeV/c^2. In figure (a) the $D^\circ \to K^-\pi^+$ signal at 1.8645 GeV/c^2 and the satellite peak from the $D^\circ \to K^-\pi^+(\pi^\circ)$ decay mode are shown. The $D^\circ \to K^-\pi^+\pi^-\pi^+$ signal for $X_E > 0.4$ is shown in figure (b).

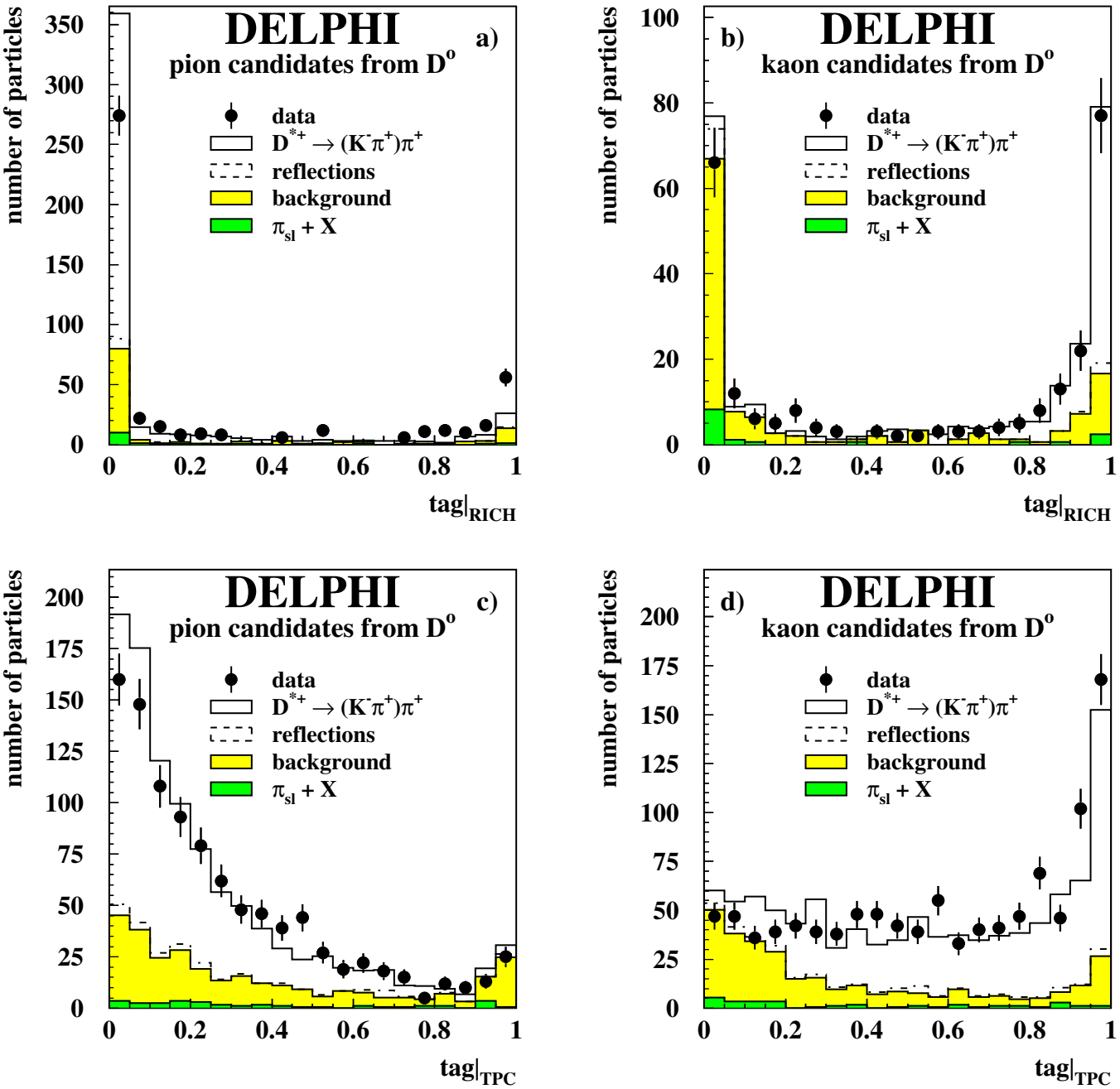

Figure 3: The particle identification obtained from the RICH information and the dE/dx measurement in the TPC. The separation between pions and kaons obtained from the RICH information is shown for a pion (a) and an enriched kaon sample (b) from $D^{*+} \rightarrow (K^-\pi^+)\pi^+$ decays. The corresponding distributions provided by the dE/dx measurement of the TPC are shown in figures (c) and (d), respectively. See section 4 for the definition of $tag|_{RICH}$ and $tag|_{TPC}$.

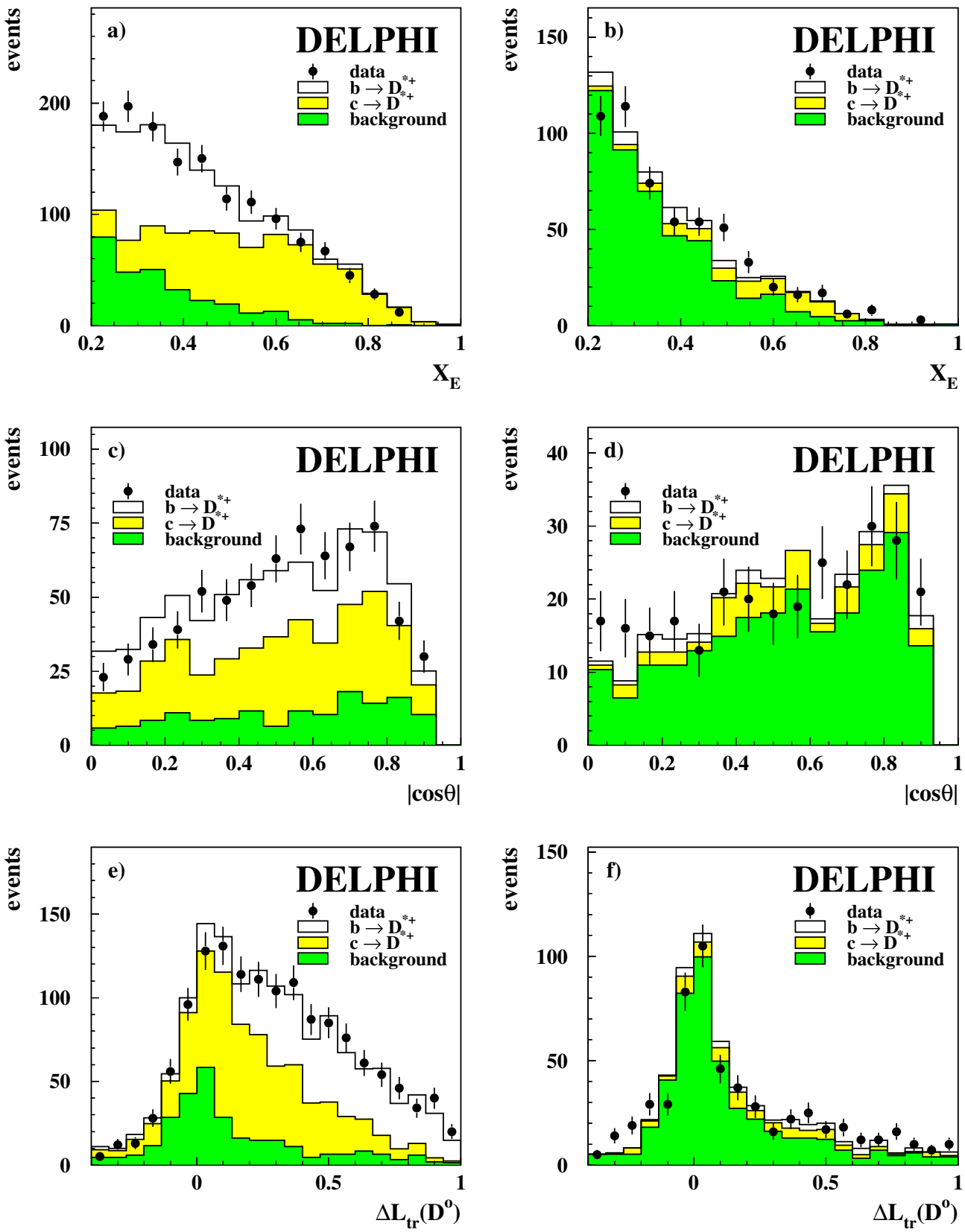

Figure 4: The scaled energy (a+b), polar angle (c+d) and transformed decay length (e+f) distribution for the $D^{*+} \to (K^-\pi^+)\pi^+$ decay mode. The signal region (left) is selected by the Δm interval between 0.1435 GeV/c^2 and 0.1475 GeV/c^2, while for the sidebands (right) the interval 0.1475 GeV/$c^2 < \Delta m < 0.1525$ GeV/c^2 is used. The data are compared with simulation where D^{*+} from charm and bottom events and combinatorial background are shown separately. See section 5.1 for the definition of the scaled decay length ΔL_{tr}.

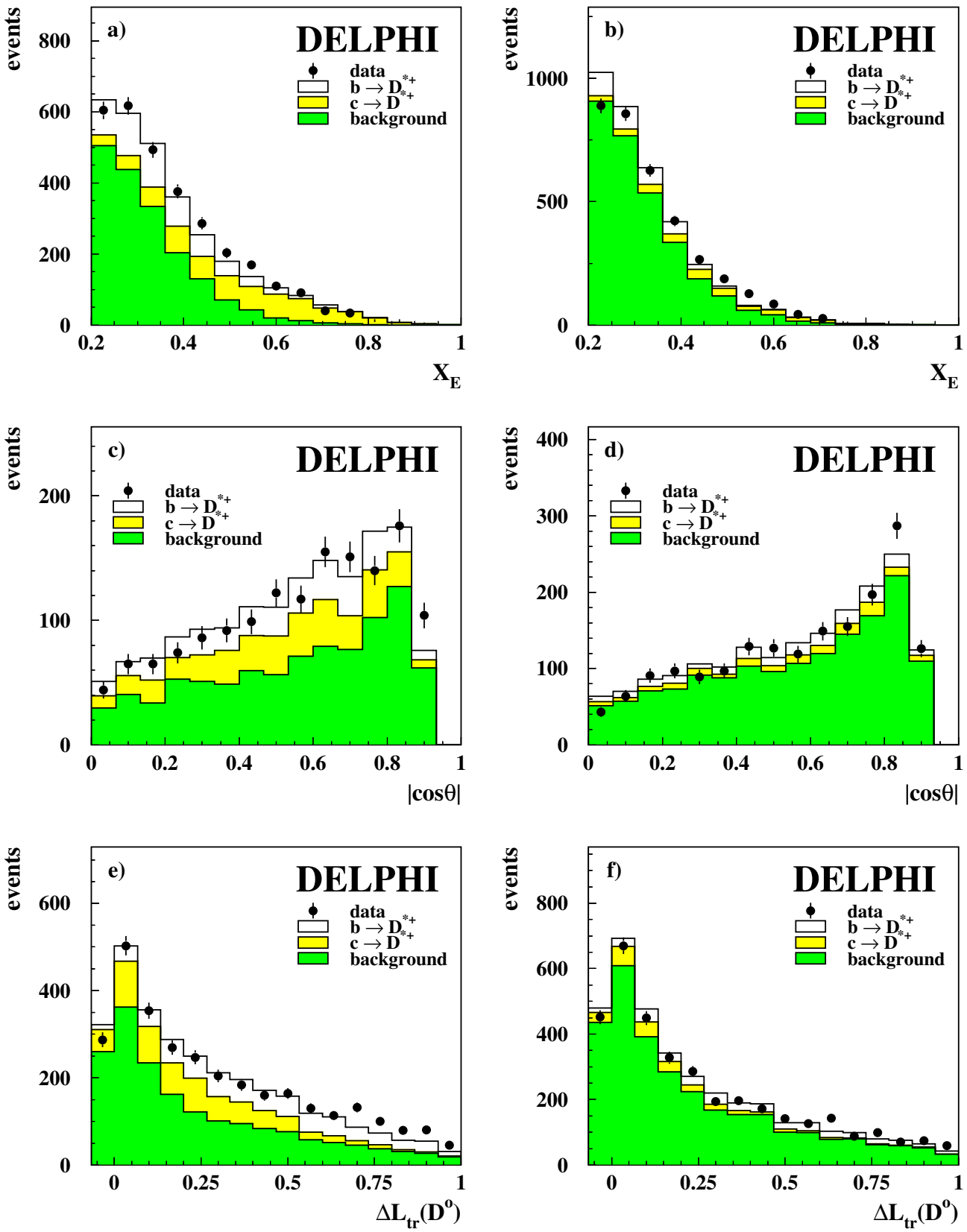

Figure 5: The $D^{*+} \rightarrow (K^-\pi^+\pi^-\pi^+)\pi^+$ decay mode as in figure 4. The same Δm intervals are used to define the signal and sideband regions.

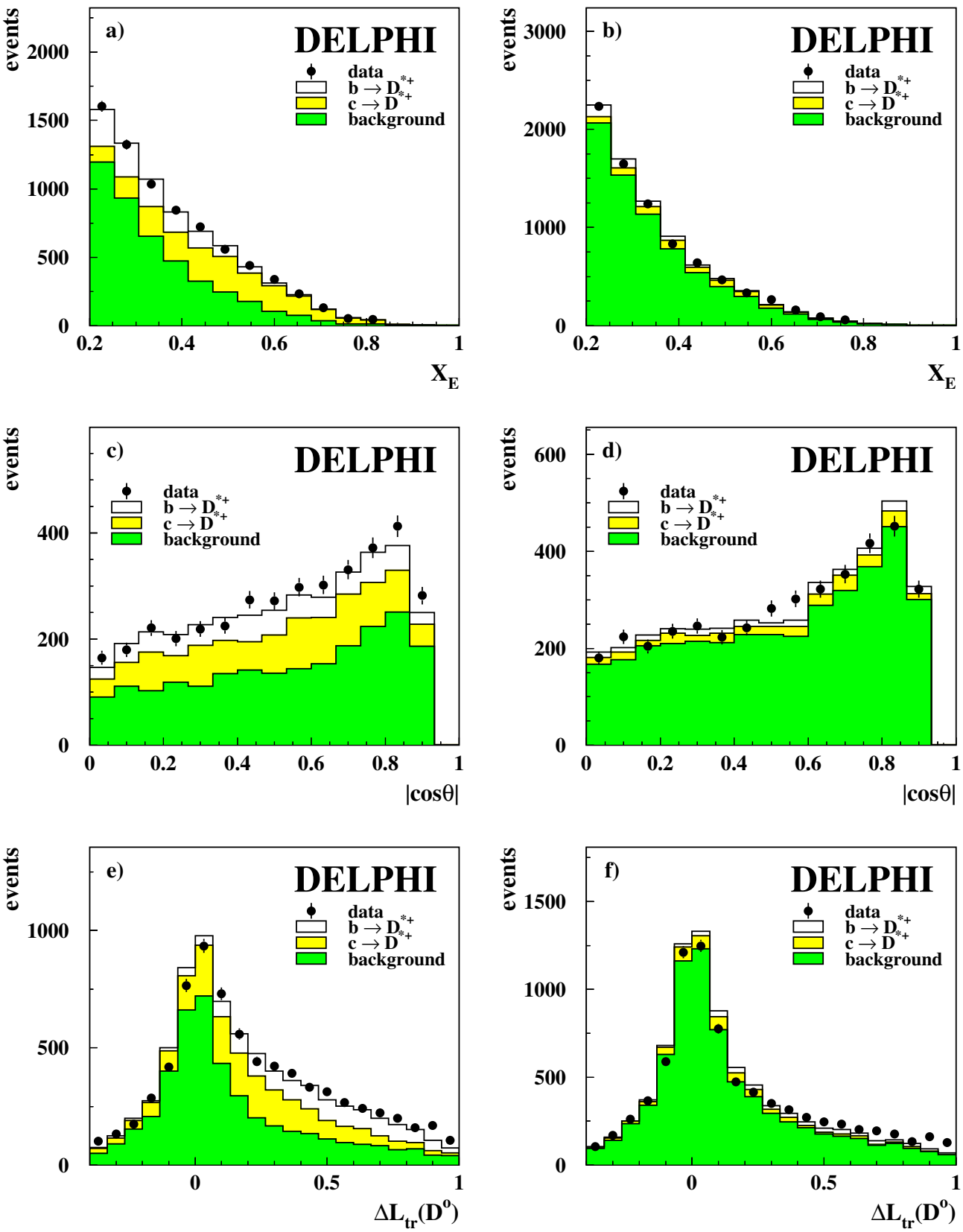

Figure 6: The $D^{*+} \to (K^-\pi^+\pi^\circ)\pi^+$ decay mode as in figure 4. Since the signal is broader in this decay mode, the intervals $\Delta\mathrm{m} < 0.155\ \mathrm{GeV}/c^2$ and $0.155\,\mathrm{GeV}/c^2 < \Delta\mathrm{m} < 0.170\ \mathrm{GeV}/c^2$ are used to define the signal and sideband regions, respectively.

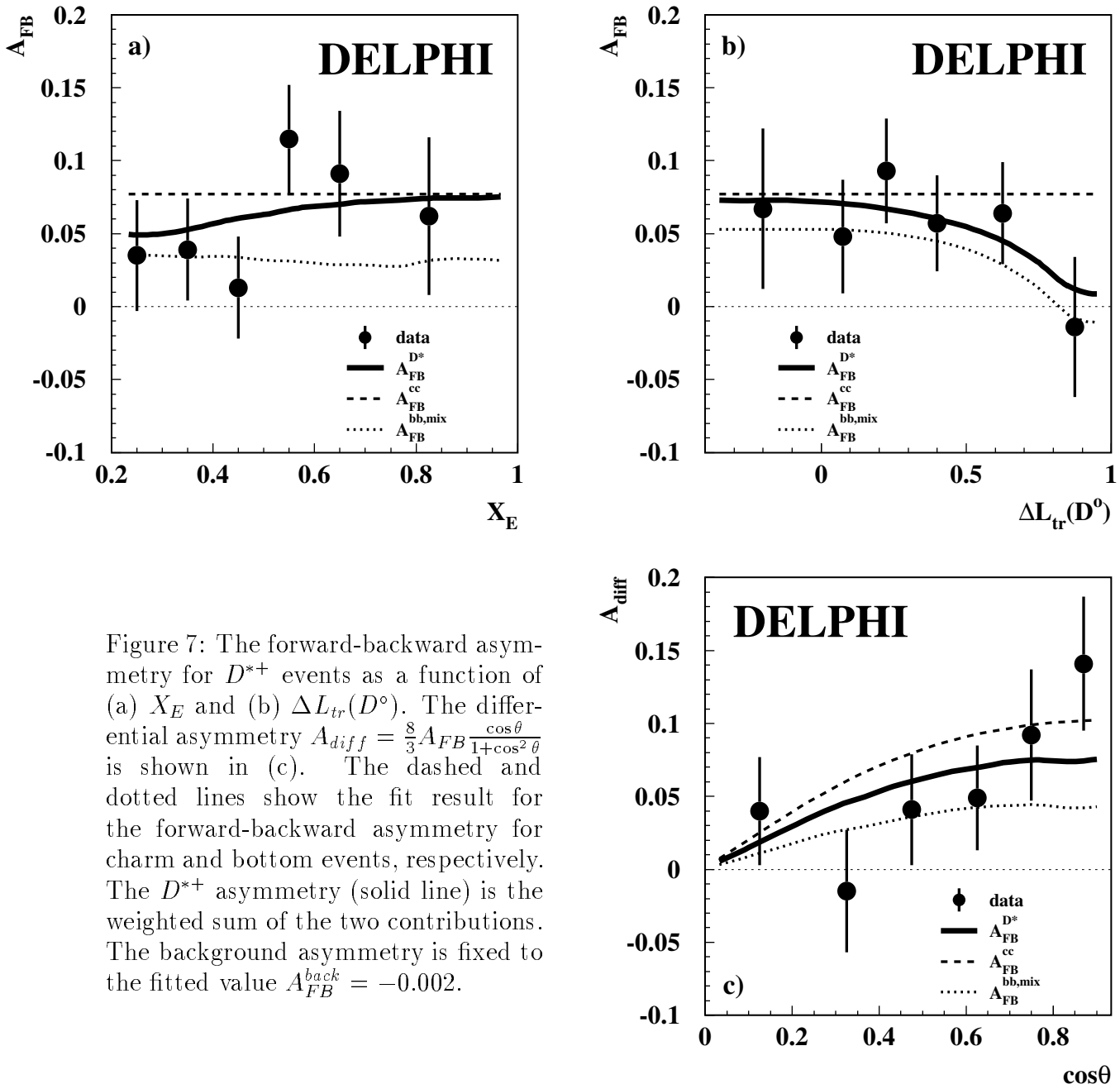

Figure 7: The forward-backward asymmetry for D^{*+} events as a function of (a) X_E and (b) $\Delta L_{tr}(D^\circ)$. The differential asymmetry $A_{diff} = \frac{8}{3} A_{FB} \frac{\cos\theta}{1+\cos^2\theta}$ is shown in (c). The dashed and dotted lines show the fit result for the forward-backward asymmetry for charm and bottom events, respectively. The D^{*+} asymmetry (solid line) is the weighted sum of the two contributions. The background asymmetry is fixed to the fitted value $A_{FB}^{back} = -0.002$.